

# Ionospheric Precursors of the Intensification of Isolated Tropical Cyclones According to the IKB-1300 and Cosmos-1809 Satellite Data

V. M. Kostin<sup>a, c</sup>, G. G. Belyaev<sup>a</sup>, B. Boichev<sup>b</sup>, E. P. Trushkina<sup>a</sup>, and O. Ya. Ovcharenko<sup>a</sup>

<sup>a</sup> Pushkov Institute of Terrestrial Magnetism, Ionosphere, and Radiowave Propagation, Russian Academy of Sciences (IZMIRAN), Troitsk, Moscow oblast, 142190 Russia

<sup>b</sup> Institute of Space Research and Technologies, Bulgarian Academy of Sciences, Sofia, Bulgaria

<sup>c</sup> State University of Management, Moscow, Russia

e-mails: belyaev@izmiran.ru; boytchev@bas.bg; kostin@maryno.net

Received July 2, 2014; in final form, August 18, 2014

**Abstract**—The ionospheric parameters were analyzed, which made it possible to distinguish several successive stages in the development of isolated tropical cyclones (TCs). Data were taken from the Cosmos-1809 and Intercosmos Bulgaria-1300 satellites, which passed over several dozen TCs. The first stage of TC development consists of a sharp increase in altitudinal substorm activity caused by a tropical disturbance and depression. During this stage, plasma density caverns extending over several hundreds of kilometers are observed in the nighttime upper ionosphere a day before the formation of a tropical storm or even a category-I hurricane. The second stage, typical of TCs with intensities reaching categories I and II, is the displacement of a wide plasma density maximum in the upper ionosphere from the geomagnetic equator into the region, the center of which along the geomagnetic field line is projected to 200–230 km altitudes at a TC latitude. The third stage, which is typical of TC categories III–V, consists of the formation of an additional  $Ne$  peak (with a width reaching 1000 km) near the TC zenith. This peak includes  $\Delta Ne$  disturbances and is accompanied by electrostatic oscillations at the  $H^+$  and  $He^+$  cyclotron frequencies and at the lower hybrid resonance frequency and by electric fields that are projected into the magnetically conjugate region. The crossing of New Caledonia by the category-IV TC Harry was considered in detail. It was shown that the neutral particle ascending jet probably deviated along the meridian in this case.

DOI: 10.1134/S0016793215020127

## 1. INTRODUCTION

The main physical processes resulting in the formation of hurricanes and typhoons are rather well known (see, e.g., Golitsyn, 2008; Holton et al., 2003). The World Meteorological Organization (WMO) provides information about cyclones that was obtained at the centers, which control cyclone dynamics. A satellite system network has been deployed. All of these materials and references can be found on the sites <http://www.wmo.int>, <http://climate.gsfc.nasa.gov>, <http://www.nhc.noaa.gov/climo>, and <http://www.usno.navy.mil>. The references presented below are only for top-priority works.

Unfortunately, meteorologists ignore the effect of the ionosphere on cyclonic processes, considering these processes to be small-scale. At the same time, Danilov et al. (1987) indicated that the ionosphere is a sensitive indicator of powerful meteorological processes. Several works previously considered the electric field above sources of powerful thunderstorm discharges and the propagation of this field into the ionosphere (Kelley et al., 1985; Hegai et al., 1990; Pulinets et al., 2000; Isaev et al., 2002). The effect of

thunderstorm activity and arising internal gravity waves on the ionosphere was considered at several international conferences. For example, the materials of one of these conferences are presented in the special issue of *Journal of Atmospheric and Solar–Terrestrial Physics (Effects ...)*, 1998). The role of electromagnetic interactions in the dynamics of atmospheric vortices was discussed in (Artekha et al., 2003, 2013).

The structure of the ionosphere above TCs is studied by means of rocket sounding (Vanina-Dart et al., 2008) and tomographic sounding from low-orbiting satellites (Vanina-Dart et al., 2011) and GPS (Zakharov and Kunitsyn, 2012; Zakharov et al., 2012). It was previously indicated that ELF–VLF oscillations above TCs are modified in much wider regions than the electric field penetration zone (Mikhailova et al., 2002). A postevent analysis of the Cosmos-1809 complex measurements of the ELF–VLF oscillations, plasma density and temperature, and electric fields indicated (Isaev et al., 2010; Belyaev et al., 2011, 2012) that the effect of TCs on the ionosphere is much more complex than the addition to the IRI model (Araujo-Pradere et al., 2003).

It was shown that a TC is intensified at a high temperature of the surface ocean water,  $t > 26^{\circ}\text{C}$  (Holton et al., 2003). It is assumed that an increase in the number of condensation centers is an additional factor in TC intensification. Aerosols, continental dust (e.g., a dust storm in the Sahara caused the Izabel hurricane (2003)), or ions during the ionization of atmospheric gases by energetic particles of a different origin (Veretenenko and Pudovkin, 1996; Krivolutskii and Repnev, 2012) are such centers. Thus, Bondur et al. (2008) consider that the intensification of the Katrina hurricane (2005) was caused by an increase in the galactic cosmic ray flux. Such a change may be caused by a magnetic storm (Ivanov, 2006, 2007).

The aim of this work is to search for possible precursors of the intensification of isolated TCs. An altitudinal anticyclone is formed above the depression center in the tropopause when a TC is self-organized. An ascending jet of neutrals (convection) successively reaches the altitudes of the *D*, *E*, and *F* layers and higher altitudes. Precursors of isolated TC can be found in the ionosphere in these cases. We should note that the *Ne* structures in the ionosphere change differently for interacting TCs, e.g., the Page and Owen typhoons of category V (1990) (Kostin et al., 2011).

## 2. INITIAL EXPERIMENTAL DATA AND MAIN RESULTS

The Intercosmos-Bulgaria-1300 satellite with 11 onboard devices, which are used to study physical processes in the ionosphere and magnetosphere, was designed in Bulgaria. The satellite was launched on August 7, 1981, into orbit with an apogee of  $\sim 900$  km, a perigee of  $\sim 800$  km, and an inclination of  $81.3^{\circ}$ . It functioned until 1983. This was the first satellite of the Intercosmos series with triaxial stabilization, which provided good time resolution.

The Intercosmos-Bulgaria-1300 satellite measurements were in unique, because they were performed in years of very high solar activity. Ten years later, another satellite (Cosmos-1809) also operated in years when solar activity was maximal (from December 18, 1986, to May 23, 1993). The satellite orbit parameters were as follows: the apogee was 980 km, the perigee was 950 km, the inclination was  $82.5^{\circ}$ , and the period was 104 min. Since the satellite was synchronized with respect to the Sun, all nearby orbits had identical ionospheric illumination intensities.

A series of tropical hurricanes was observed in the Atlantic Ocean in August and September 1981. The active phase of the strongest of these hurricanes (the category-IV Harvey hurricane) was registered on September 11–19. The hurricane maximal velocity was  $\sim 215$  km/h, and the pressure drop was 946 hPa. In this region hurricanes usually develop from tropical waves that originate above the anticyclone in West Africa.

Figures 1 and 2 show the results achieved from the Intercosmos-Bulgaria-1300 satellite with regard to tropical wave development dynamics (the tropical depression and storm) up to the hurricane stage and its breakdown. The data of the density (*Ni*, *Ne*) measurements are presented on the logarithmic scale, and those of the *Te*, satellite potential, and VLF–ELF oscillation measurements, registered in the narrowband channels at frequencies of 140, 1200, and 4900 Hz, are presented in telemetric volts.

Panel (a) of Fig. 1 for August 29, 1981, reflects tropical wave generation. It is evident that the *Ne* bursts and *Ni* troughs (a thick line) at  $L = 1.25$  are registered above the anticyclone in West Africa.

Trapped whistlers caused by electric charges in a dust storm cloud were apparently observed at  $L = 1.25$ . Such a viewpoint is qualitatively confirmed by *Ni* caverns without a synchronous change in *Te*, bursts in the E-4900 Hz VLF–ELF channel, a suppression of oscillations in the E-140 Hz ELF channel, or a satellite potential drop in the magnetically conjugate region.

A typical density trough near the magnetic equator corresponds to the reconstruction of the ionosphere behind the evening terminator during high solar activity ( $F10.7 \sim 260$ ).

Panel (b) of Fig. 1 corresponds to the beginning of the Harvey hurricane decay. The wind velocity in the cyclone decreased to 110 km/h, and the pressure increased to 995 hPa. The archived data (<http://www.nhc.noaa.gov/climo>) indicate that a powerful anticyclone was formed in the stratosphere above the Harvey hurricane on September 11–15, 1981. During two days after this event, the hurricane center ( $36.8^{\circ}$  N,  $50.6^{\circ}$  W) moved northward from the altitudinal anticyclone ( $\sim 30^{\circ}$  N), at a latitude at which ( $L = 1.5$ ) *Ne* fluctuations were observed. As on panel (a), these fluctuations could apparently be caused by intense lightning discharges, which were accompanied by showers before the typhoon decay (Mikhailova et al., 2002). The satellite potential usually considerably decreases in this region, which can be caused by the penetration of an ascending neutral flux to altitudes of the upper ionosphere (Isaev et al., 2010). An additional *Ni* peak at  $L = 1.23$  is possibly related to plasma removal from the ionospheric *E* region to altitudes of the upper ionosphere. This effect was analyzed in detail in (Isaev et al., 2010).

We should note that the hurricane effect weakens and “bubbles” ( $L = 1.23$ ), where *Te* synchronously decreases and electrostatic oscillation bursts in the 140 Hz channel, including the  $\text{He}^+$  frequency are registered, develop in the conjugate hemisphere. An abrupt decrease in the  $\text{He}^+$  concentration in bubbles was shown in (Sidorova and Filippov, 2013).

In September 1981 the Harvey hurricane weakened and entered the tropical storm stage, and the hurricane effect on the ionosphere decreased. Therefore, strong bubbles are observed on both sides of the geo-

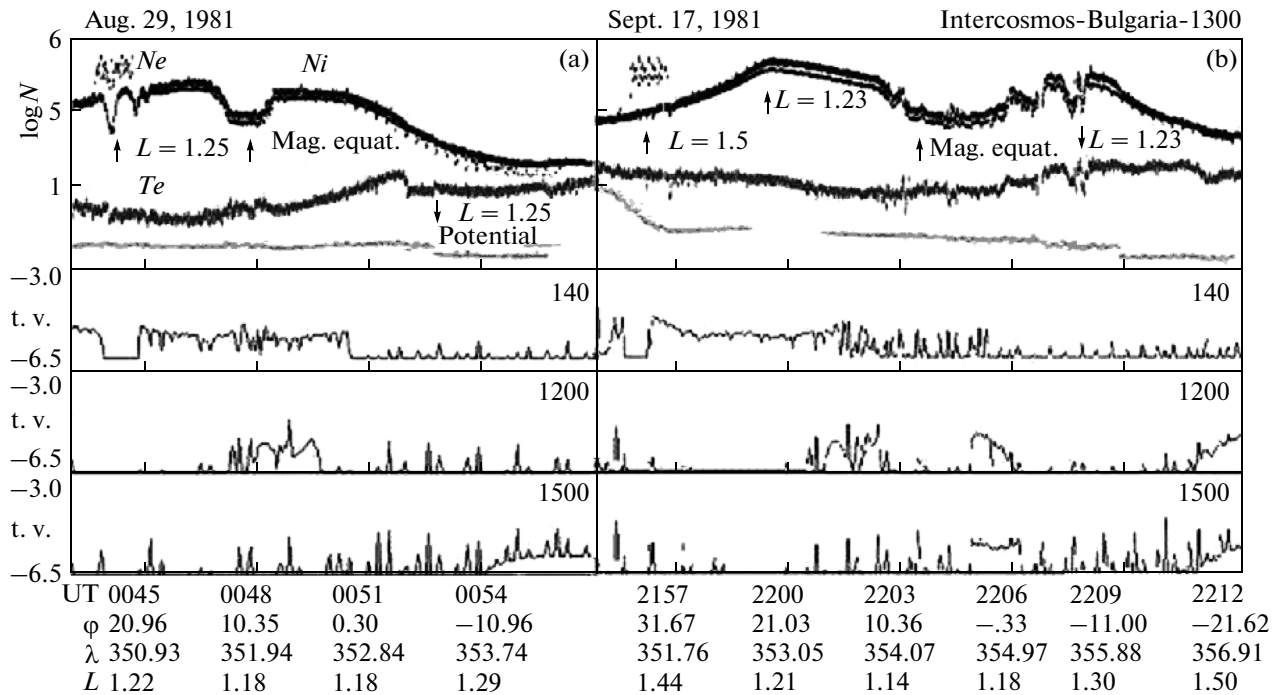


**Fig. 1.** (a) Origination of the Harvey hurricane over Western Sahara ( $L = 1.25$ ); (b) the electron component fluctuations at the latitude of the high-altitude anticyclone center above the hurricane ( $L = 1.5$ ).

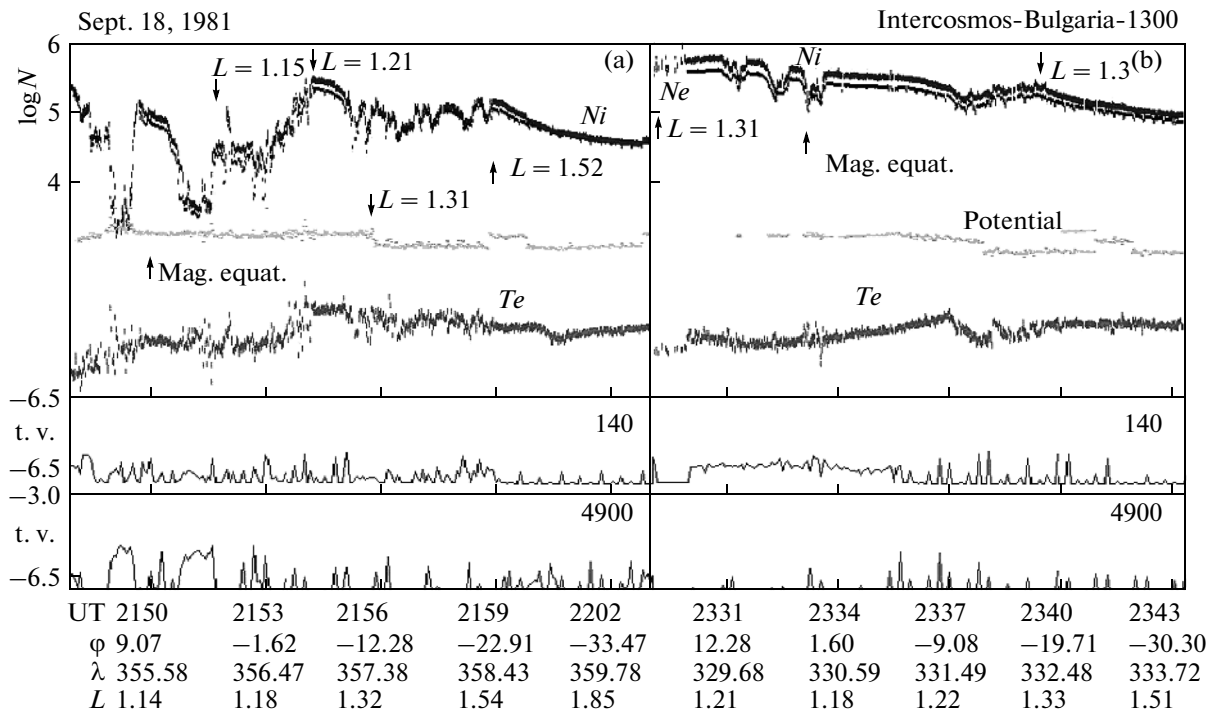


**Fig. 2.** Influence of the Harvey hurricane ( $38^\circ$  N,  $44^\circ$  W) and forming Irene hurricane ( $14^\circ$  N,  $30^\circ$  W) on the ionosphere.

magnetic equator (Fig. 2, panel a). Weaker density fluctuations of the small bubble type at  $L = 1.32$ – $1.54$  are observed in the magnetically conjugate region of the originating Irene hurricane (1981). A similar

anomalous electron density depression in the ionosphere above the originating Kurrily (1989) and Aviona (1992) typhoons was previously referred to in (Isaev et al., 2010; Belyaev et al., 2011).

Characteristics of TCs and the satellite position at the TC latitude

No	TCs	Lifetime	Maximal velocity	Day	$\varphi$	$\lambda$	Velocity, <i>kt</i>	Orbit	UT	$\Delta\lambda$
1	Harry	Feb. 6–22, 1989	130	10 11	19 S 21 S	165 E 163 E	110 105	10850 10864	1358 1417	2 W 6 W
2	Roslyn	Sept. 13–30, 1992	85	24	18 N	146 W	65	29116	0606	9 E
3	Ted	Sept. 14–24, 1992	65	24	34 N 36 N	122 E 127 E	40	29114 29120	0201 1257	2 E 1 W
4	Tina	Sept. 17–Oct. 11, 1992	115	24	13 N 13.5	110 W 109.5	75 65	29115 29123	0423 1732	7 E 6 E
5	Bonnie	Sept. 17–Oct. 2, 1992	90	24	37 N	51 W	75 65	29113 29121	0048 1411	1 W 10 W
6	Seymour	Sept. 17–27, 1992	75	24	24 N 23 N	122 W 123 W	55 45	29116 29123	0604 1735	7 W 7 E
7	Val	Sept. 19–27, 1992	55	24	16 N 17 N	157 E 157 E	25 30	29113 29119	0015 1115	12 W 1 E
8	TC05B	Sept. 21–25, 1992	30	24	22 N	90 E	25	29115 29121	0341 1445	2 E 11 E
9	Charley	Sept. 21–27, 1992	95	24	36 N	34 W	90	29120	1226	2 W
10	Danielle	Sept. 22–26, 1992	55	24	34 N	73 W	40	29114 29121	0233 1410	6 W 11 E
11	Ward	Sept. 23–Oct. 7, 1992	95	24	12 N	167 W	25	29118	0934	1 E
12	Aviona	Sept. 25–Oct. 1, 1992	65	24	4 S	84 E	15	29114 29122	0333 1637	7 E 7 W

Panel (b) of Fig. 2 shows the next orbit on September 18, 1981, which was closer to the Harvey tropical storm center and farther from the Irene originating storm. It is clear that the density fluctuates above the tropical storm center ( $L = 1.33$ ), bubbles are suppressed near the geomagnetic equator, and the  $Ne$  density and temperature anomalously behave in the magnetically conjugate region ( $L = 1.22–1.33$ ). Bubbles were completely suppressed in the next orbit, which passed west of the magnetic meridian, crossing the Harvey tropical storm (Belyaev et al., 2012). The bubble suppression effect in the ionosphere was also observed by the authors during the operation of the Sura heating facility west of its meridian (Kostin et al., 2013).

The data of the Cosmos-1809 devices were most informative for the studied problems. Electron density measurements with the impedance sonde (IS-2) were of special importance (Komrakov et al., 1970). The table presents information about individual typhoons, during the existence of which the satellite data on the ionospheric parameters discussed in the paper were obtained.

The position of typhoons and their characteristics are presented on the sites of Joint Typhoon Warning Center and National Hurricane Center. A typhoon characteristic, such as a surface wind velocity, is presented in terms of knots (nautical mile per hour), i.e.,

$1 \text{ kt} = 1.852 \text{ km/h}$ , as is accepted in meteorology. The distance from the closest satellite working trajectory from the typhoon center is given in the last column.

Figure 3 shows a unique case: a series of the satellite orbits with electron density registered when 11 typhoons were observed in one day (September 24, 1992). The typhoon position is marked by heavy points on the TC trajectories (see table).

The first descending circuit (circuit 1) in Fig. 3 corresponds to orbit 29113; the first ascending circuit corresponds to the end of orbit 29113 and the beginning of orbit 29114. In the evening sector (LT = 2140), the solar shadow was above the satellite, beginning from a latitude of  $45^\circ \text{ N}$  downward. The magnetic flux tube vertices were in the shadow at  $L < 1.8$ .

In the Atlantic and eastern Pacific, the mapped typhoons, except Bonnie, were caused by tropical waves that started from Africa from August 31 to September 8. In the Indian Ocean and western Pacific, typhoons were formed from the monsoon trench.

An analysis of the  $Ne$  records in Fig. 3 and typhoon trajectories makes it possible to draw the following conclusions.

(i) The shift of the  $Ne$  maximum in the Northern Hemisphere from the  $230^\circ \text{ E}$  meridian to the  $270^\circ \text{ E}$  meridian during 10 h may be apparent, since the Tina typhoon weakened and the Charley typhoon intensi-

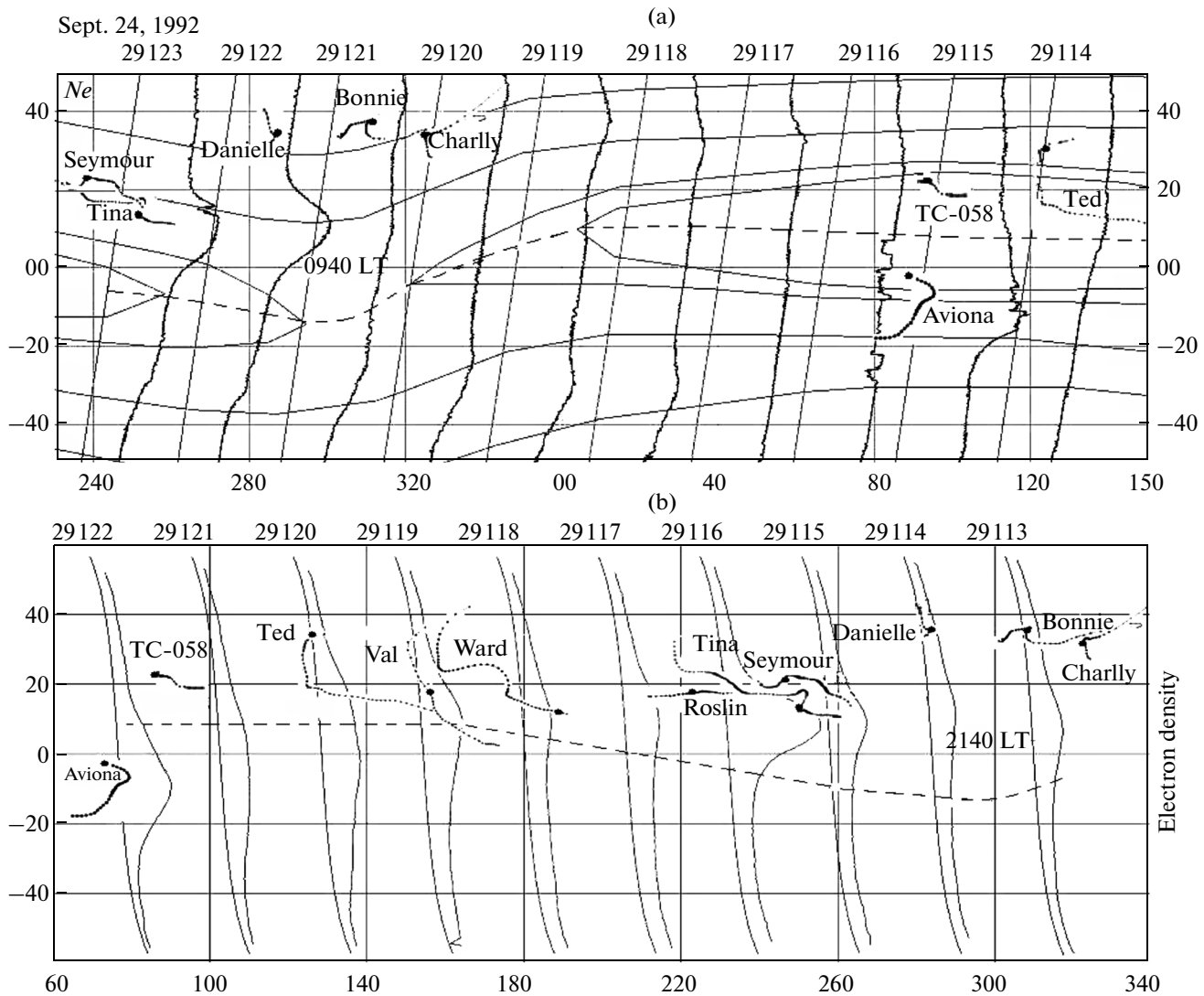


**Fig. 3.** Electron density (thick lines) in the morning and evening sectors at  $h = 960$  km during the simultaneous development of 11 TCs. The geomagnetic equator is marked by a dashed line.

fied. This fact confirms that the effect of typhoons on the ionospheric parameters is considerable.

(ii) The position of the equatorial global ionospheric  $Ne$  maximum at the  $80^{\circ}$ – $90^{\circ}$  E meridian in the Southern Hemisphere insignificantly changes over 12 h.

(iii) On that day, all typhoons in the Atlantic water area sharply changed their trajectories, which corresponds to the average time during which the summer stratospheric circulation changes into the winter circulation (Gabis and Troshichev, 2011).

(iv) The localized electron density caverns in orbit 29116 near the Aviona typhoon, which were formed a day before the typhoon intensification, apparently promote a change of the tropical depression (the wind above the ocean is  $<25$  kt) into the hurricane state.

(v) Electron density caverns have a small-scale internal structure and are often filled with ELF elec-

trostatic oscillations at a frequency of  $f = 140$  Hz (Belyaev et al., 2011).

(vi) An additional  $Ne$  maximum above the Tina category-II hurricane is observed before the hurricane intensification to category IV (orbit 29123). The  $\Delta Ne$  fluctuation structure in the vicinity of an additional  $Ne$  maximum is similar to the structure of the isolated peak above TC Harry (1989) before this cyclone crossed New Caledonia (see below, Fig. 5, orbit 10850).

Isaev et al. (2010) considered in detail the ionospheric parameters in the vicinity of category-IV TC Harry. The cyclone trajectory was constructed based on the [www.meteo.nc/cyclone/](http://www.meteo.nc/cyclone/) site data and is shown in Fig. 4.

Figure 5 presents the electron density ( $Ne$ ) parameters in individual orbits. The electric field values ( $E_y$ ) obtained with a partially open sensor rod, which

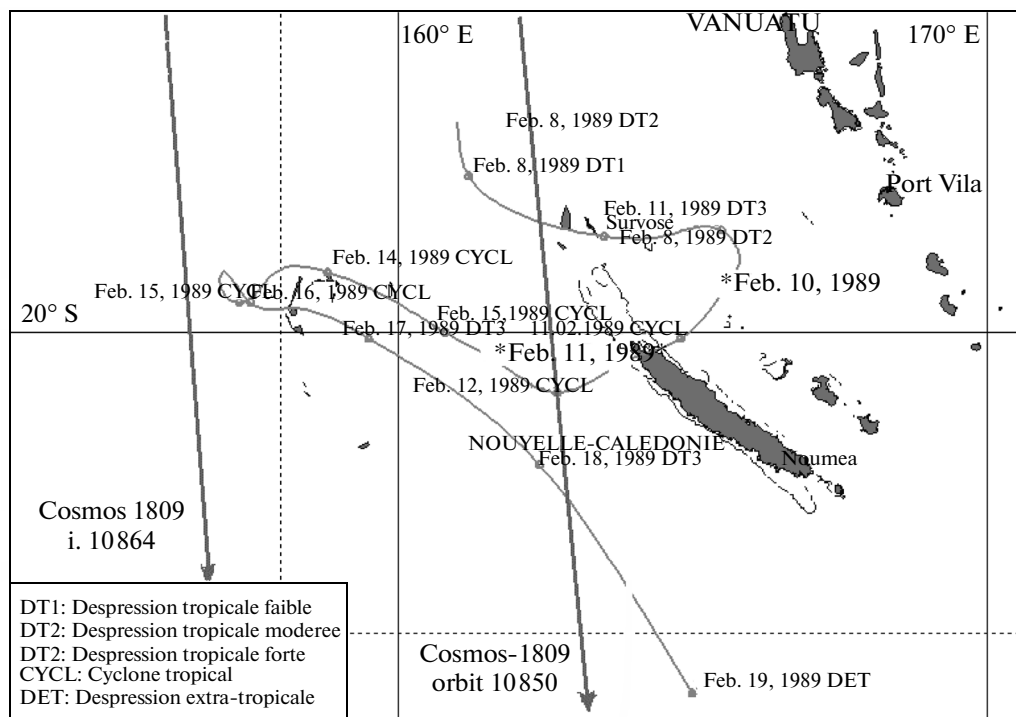


**Fig. 4.** Harry cyclone trajectory and the closest orbits of Cosmos-1809. The TC position is marked by asterisks with the corresponding date.

makes it possible to qualitatively estimate the field longitudinal component, are presented in addition to the data from (Isaev et al., 2010).

A principal singularity—an additional  $N_e$  peak with a width of  $\sim 800$  km—is registered in orbit 10850, which is the closest orbit to TC on the Harry latitude (the distance from the TC center ( $\sim 2.8^\circ$ ) is marked by a vertical arrow on the lower panel). The following singularities are observed in the peak structure.

(i) A narrow emission peak in the ELF channel at  $f = 140$  Hz, including  $\text{He}^+$  cyclotron frequency.

(ii) The  $N_e$  fluctuations are  $\sim 2\%$ ; the density fluctuation period within the peak is twice as short as the period outside the peak, where  $\lambda \sim 150$  km.

(iii) A wide emission maximum in the channel at  $f = 4600$  Hz, which is projected along the geomagnetic field line up to an altitude of  $\sim 200\text{--}230$  km at the TC “eye” latitude. Lower hybrid plasma oscillations fall within this frequency range when  $\text{O}^+$  ion concentrations increase.

(iv) The transverse electric field (the  $E_x$  component) smoothly increases from the emission maximum region at  $f = 4600$  Hz to the  $N_e$  maximum and abruptly drops, which corresponds to the disturbance vertical source.

(v) The longitudinal electric field in the unlit ionosphere is not detected. Singularities in the  $E_y$  component are absent. The solar shadow above the ( $163^\circ$  E,

$20^\circ$  S) point was at altitudes of  $H = 3920, 4560,$  and  $2110$  km at 1214, 1358, and 1443 UT, respectively. Hydrogen ionization by the scattered radiation in the  $H$  line can be an additional electron source in the nighttime ionosphere (Danilov, 1989).

The indicated ionospheric singularities above TC Harry are modified the next night, when New Caledonia is crossed (Fig. 6).

The main structural formations caused by the TC effect in the ionosphere are marked by arrows. The numerals correspond to the following  $L$  shells:

$L = 1.48$ : the projection on the TC center latitude, where  $\text{H}^+$  and  $\text{He}^+$  cyclotron oscillations are intensified;  $L = 1.82$ : the center of the  $N_e$  additional peak with a width of  $\sim 800$  km;  $L = 1.2$ : the main  $N_e$  maximum shifted from the geomagnetic equator;  $L = 1.31$ : the  $N_e$  maximum, which is projected along the geomagnetic field line onto the TC latitude, reaches altitudes of  $h = 200\text{--}230$  km; g.e. indicates that the satellite passed over the geomagnetic equator.

Individual anomalous bursts of ELF–VLF emissions are marked by additional arrows with the abbreviations of VLF transmitters. An upward arrow corresponds to the situation when the satellite crossed the  $L$  shell resting on the transmitter latitude in the lower ionosphere; downward arrows correspond to the  $L$  shells in the conjugate ionosphere. Only VLF transmitters located at a distance of  $\sim 10^\circ$  along longitude, where magnetospheric signals are usually detected, are

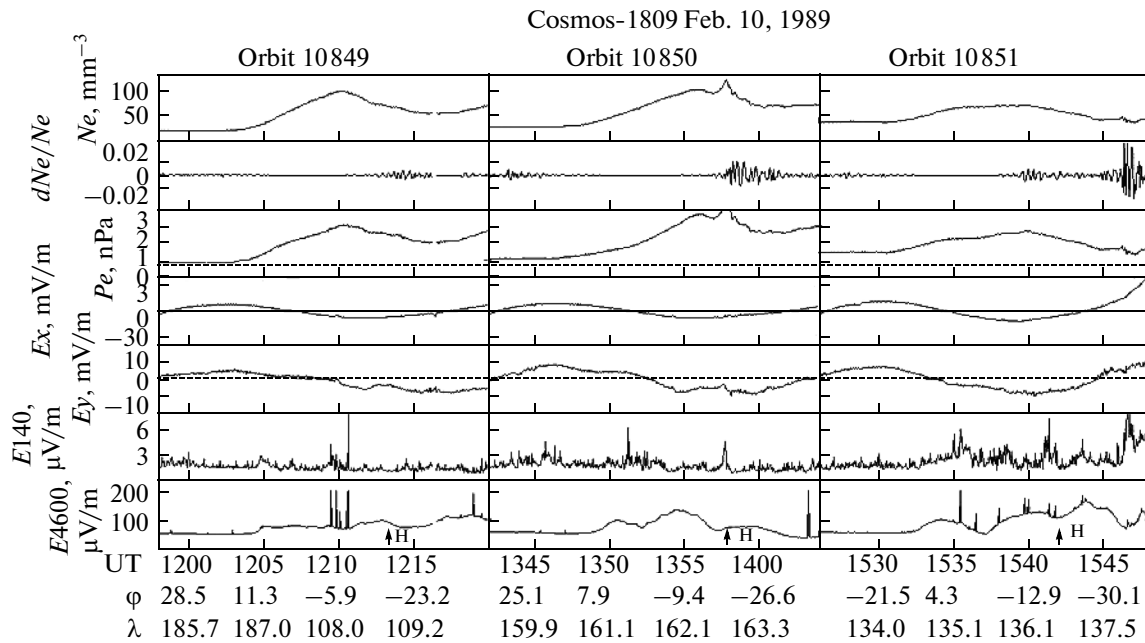


**Fig. 5.** Plasma parameters ( $h = 960$  km) of the nighttime ionosphere (LT = 0036) before the situation when TC Harry crossed New Caledonia.

shown (Molchanov, 1985). Joint studies, performed on the Cosmos-1809 and DE-1 satellites above the RA-3 transmitter (Komsomolsk-on-Amur), indicated that a duct filled with energetic particles and ELF emissions was observed at the  $L = 2.94$  shell (Sonwalkar et al., 1994).

We should note that the TC intensity decreased to the category-II level when New Caledonia was crossed and then started increasing to the category-IV level (Fig. 7).

The denotations in Fig. 7 are the same as in Fig. 6. The solar shadow above the ( $163^\circ$  E,  $20^\circ$  S) point was at altitudes of  $H = 1890, 4444, 4233, 1688,$  and  $274$  km at 1051, 1235, 1419, 1603, and 1747 UT, respectively.

An analysis of the ionospheric plasma parameters in the situation when TC Harry crossed New Caledonia makes it possible to draw the following conclusions.

(i) The behavior of the electric field  $E_y$  component above the typhoon in orbit 10860 is apparently explained by an ascending flow in the neutral atmosphere, which carries ions upward as a result of collisions. In this case plasma quasi-neutrality is maintained by the electron mobility along the geomagnetic field. The  $E_y$  component starts increasing on a flux tube resting on the  $E$  region above the typhoon.

(ii) A joint analysis of the  $E_x$  and  $E_y$  components confirms the conclusion that plasma drifts eastward.

(iii) Anomalous thunderstorm activity is observed in the eastern and western typhoon peripheries (orbits 10859 and 10861). Abrupt emission bursts in the chan-

nels at  $f = 4600$  and  $450$  Hz originate as a result of unducted whistlers.

(iv) The reflection of whistlers at altitudes of 2000–3000 km in the nightside magnetosphere, where hydrogen predominates, apparently causes electrostatic turbulence near the hydrogen cyclotron frequency, which extends up to the satellite altitude. The signal is intensified in the channel at  $f = 450$  Hz, the bandwidth of which includes the hydrogen cyclotron frequency.

(v) Additional channels of the IZ-2 device with the  $\Delta Ne$  fluctuation fine structure indicate that Langmuir turbulence reaching  $\sim 10\%$  is observed over a wide region ( $\geq 1000$  km) along the meridian above the typhoon. This anomaly is reflected in the noise level in the electron part of the whistler branch, which is registered in the  $f = 15000$  Hz channel.

(vi) We can judge a change in the plasma ion composition above the typhoon based on the noise asymmetry near the lower hybrid frequency in the  $f = 4600$  Hz channel in the Northern and Southern hemispheres.

### 3. POSSIBLE MECHANISMS BY WHICH AN ISOLATED STRONG TC AFFECTS THE IONOSPHERE

We can combine the experimental data presented above, based on the assumption that a TC becomes more self-organized when the neutral vertical transport increases. Initial TC development is limited by the tropopause. The vertical flow will substantially intensify when the air in the stratosphere above TC

Cosmos-1809 Feb. 11, 1989

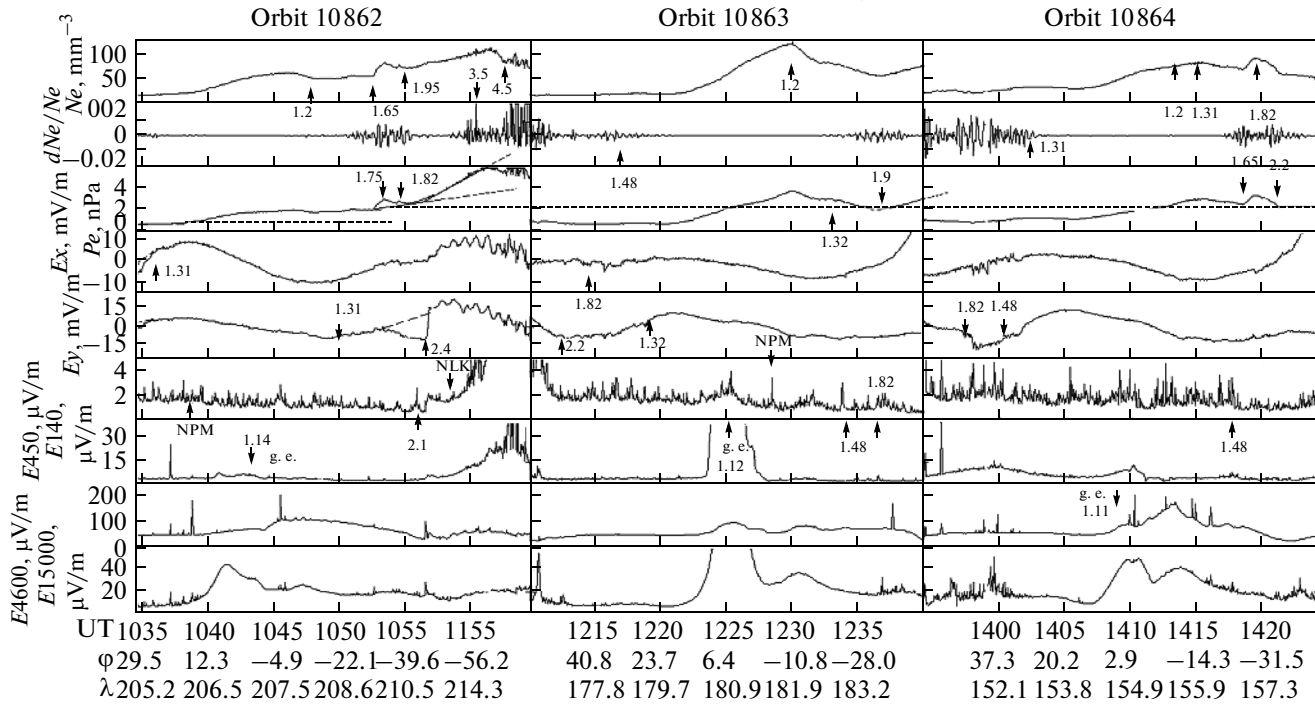


Fig. 6. Modification of plasma in the eastern sector of the nighttime ionosphere (LT = 0027) when TC Harry crossed New Caledonia,  $Kp = 3$ .

warms-up and the stratospheric anticyclone is formed. High-altitude electric discharges modify the state of the mesosphere (Evtushenko and Mareev, 2011), and the arising internal gravity waves (IGWs) propagate upward. The calculations indicate that IGWs are self-organized when their amplitudes are large, and nonlinear vortex structures are formed in an inhomogeneous ionosphere (Aburjania et al., 2013). If the horizontal wind penetrates into a structure, the IGW deviates from the vertical downwind (Erokhin et al., 2012; Sorokin and Pokhotelov, 2010).

In aerodynamics and hydrodynamics, flow motion in a medium is usually considered a submerged jet (see. e.g., (Landa, 1996)). The stability of such a system is related to the generation of surface waves propagating along a jet and by the excitation of infrasonic volume waves toward a source. We will consider the ascending jet of neutrals above a stratospheric anticyclone as a vertical submerged jet.

An acoustic wave beam warms the medium as a result of the partial loss of its energy. The temperature rises, and the medium takes on lens properties (Rudenko and Sapozhnikov, 2004). If an ascending submerged jet with the boundary layer forms a blast pipe, escaping particles will accelerate. If a jet is blown by a latitudinal wind and the jet bottom part is decelerated by an island, the originating structure as a whole will deviate in the meridional direction under the action of the force moment in this case. This situation is reflected in Fig. 8.

Here we take into account the fact that the neutral gas motion above the  $\sim 230$  km altitude can be considered the motion of individual noninteracting particles escaping along ballistic trajectories, with the most probable directional velocity about  $\sim V_T = (2kT/m)^{1/2}$ . For  $T = 1000$  K, the most probable velocities are  $V_O = 1016$  m/s for oxygen,  $V_{He} = 2038$  m/s for helium, and  $V_H = 4076$  m/s for hydrogen. Oxygen, helium, and hydrogen atoms can reach altitudes of 52, 208, and 831 km, respectively, counting off from an injection altitude of  $\sim 230$  km. In the presented scheme, it is assumed that the thermal scatter of escaping particles is substantially smaller than that of the directional velocity.

To avoid figure overloading, we conditionally show escaping particles of the reverse jet boundary layer higher and southward. The directional velocity of neutral particles of the boundary layer is actually lower than the jet velocity. These particles will cross an inclined jet and will return to the same level closer to an injection region. Only particles from the jet southern boundary can fall in the boundary layer remote area.

The common expression for the distribution of each sort of escaping neutrals ( $N_n$ ) in vertical  $h$  from cross section  $S$  with initial coordinates  $x_0$  and  $y_0$  at escape instant  $t_0$  with velocity components  $v_{0i}$  for the Maxwellian distribution with vertical velocity  $u_z$  and meridional velocity  $u_y$ , can be considered using the formula

Cosmos-1809 Feb. 11, 1989

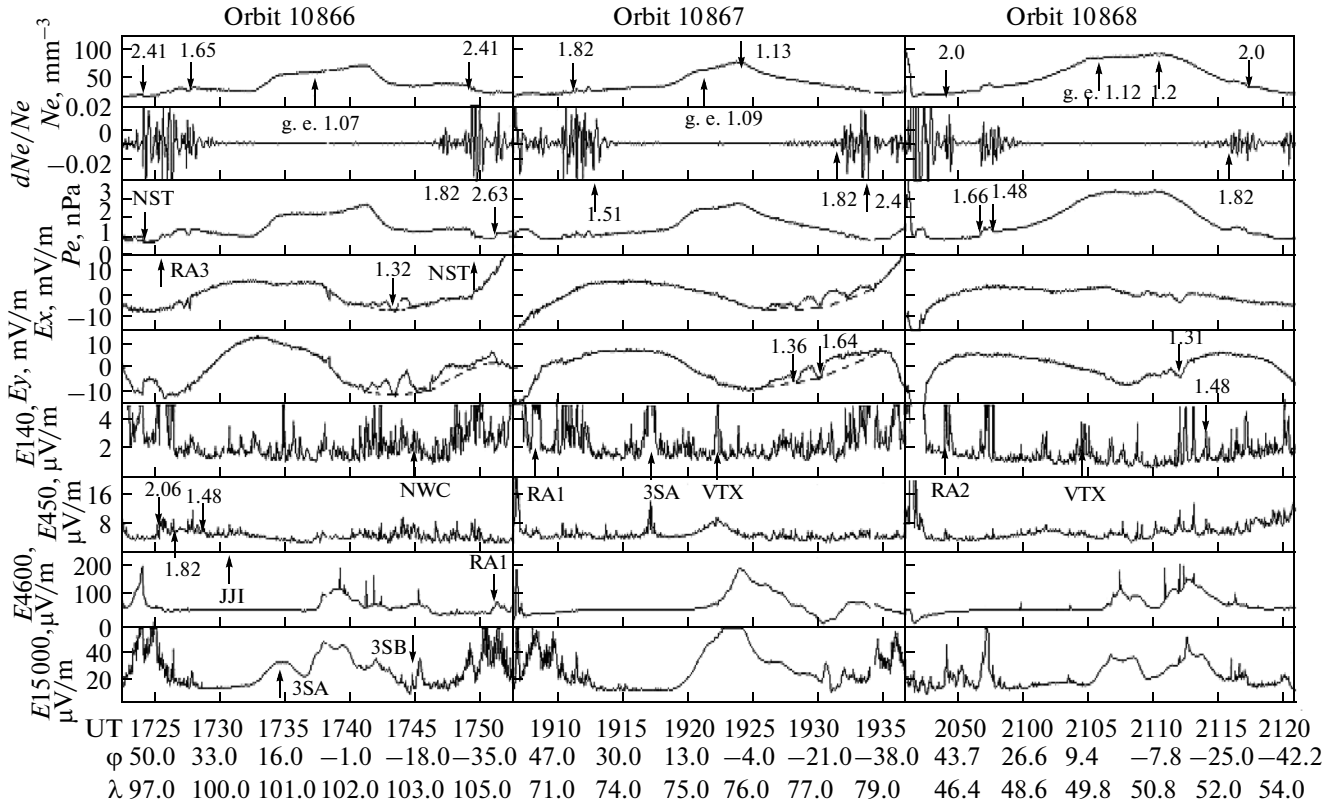


Fig. 7. Modification of plasma in the western sector of the nighttime ionosphere (LT = 0027) when TC Harry crossed New Caledonia,  $K_p = 3$ .

$$\begin{aligned}
 N_n = & \frac{N_0}{\pi^{3/2} V_T^3} \int_S dx_0 dy_0 \int_{-\infty}^t dt_0 \int_{-\infty}^{\infty} d v_{0x} d v_{0y} \int_0^{\infty} d v_{0z} \\
 & \times \delta(x - x_0 - v_{0x}(t - t_0)) \delta(y - y_0 - v_{0y}(t - t_0)) \\
 & \times \delta(h - v_{0z}(t - t_0) + \frac{g}{2}(t - t_0)^2) \\
 & \times \exp\left(-\frac{v_{0x}^2 + (v_{0y} - u_y)^2 + (v_{0z} - u_z)^2}{V_T^2}\right).
 \end{aligned} \quad (1)$$

The calculation of expression (1) is strongly simplified above the vertical quasi-monoenergetic ( $u_z \gg V_T$ ) jet with radius  $R$ . In formula (2), which is valid for  $h \leq u_z^2/2g$ ,  $N_{ef}$  is the energy of particles escaping with velocity  $u_z$ . Coefficient 2 originates due to returning particles, and the singularity in the denominator takes into account the fact that particles stop moving at apogee.

$$N_{0h} = \frac{2N_{ef} \left(1 - \exp\left(-\frac{R^2 g^2}{V_T^2 u_z^2}\right)\right)}{\left(1 - \frac{2gh}{u_z^2}\right)^{1/2}}. \quad (2)$$

If the distribution of escaping particles is Maxwellian, then integrating (2) with respect to  $u_z$ , we obtain a typical Boltzmann particle distribution over altitude in the limit of large  $R$ :

$$N_{nh} = N_0 \exp\left(-\frac{mgh}{kT}\right). \quad (3)$$

In another limiting case ( $R/h \ll 1$ ), we can indicate that the injection by a neutral hydrogen atom jet from an altitude of  $H \sim 230$  km at vertical velocities (in m/s) of

$$u_z \sim 1.5 \times 10^5 h^{1/2} T^2 R^{-2} \quad (4)$$

results in an increase in the hydrogen concentration above a TC for  $R = 200$  km and  $T = 500$  K at the Cosmos-1809 satellite altitude ( $h = 730$  km) by 10%; in this case  $u_z \sim 10^3$  m/s.

Vertical winds in the lower ionosphere with velocities reaching several hundred meters per second on scales of several hundred kilometers were observed previously (Smith, 1998). High vertical velocities in the equatorial ionosphere (up to  $\sim 10^3$  m/s) were registered for ions in bubbles (Hanson et al., 1997). It is experimentally difficult to identify narrow beams in the neutral component in the upper ionosphere with velocities close to the most probable velocity. We only consider the individual consequences of such beams,

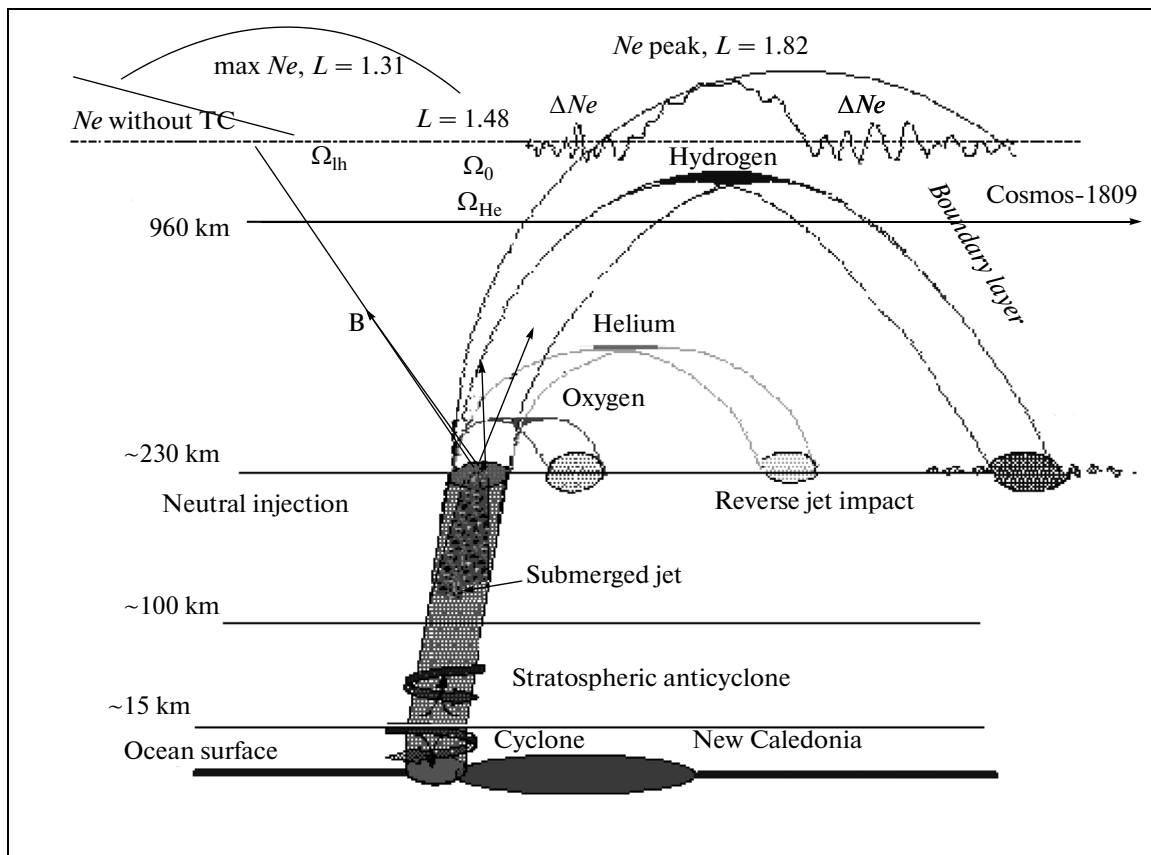


Fig. 8. The schematic influence of TC Harry on the ionosphere when this cyclone crossed New Caledonia.

which can explain the satellite observation of electromagnetic effects over TCs. We consider the following situations.

1. Intensifying TC, freely moving in the ocean.

It is known that a TC is intensified at night. Therefore, an additional  $N_e$  peak above the TC center is identified at night, when the illumination of the upper ionosphere decreases and different instabilities develop; specifically, processes of self-organization above a stratospheric anticyclone can proceed. Criterion (4) decreases if the neutral temperature in the thermosphere above a TC is higher than outside it. Such an  $N_e$  peak was observed over several TCs during the phase of their intensification from category II to category IV: Tina (1992) Fig. 4, Harry (1989) Fig. 5, and Sina (1990) (Belyaev et al., 2011). We should note that a smoothed  $N_{0h}$  singularity (2) is located below the satellite altitude ( $h_{sat}$ ), if  $u_z$  is lower than  $(2gh_{sat})^{1/2}$ . The  $N_e$  peak moves equatorward in this case.

An important singularity of the  $N_e$  peak is that the density fluctuation transverse scales outside and inside the peak differ twice, which is mentioned in the explanations to Fig. 5 and is schematically shown in Fig. 8. Such a fluctuation behavior can be explained by the

fact that both ascending and descending jets are present within the peak.

The origination of the electric field and its dependence on altitude is a characteristic indicator of the neutral jet (Fig. 5, orbit 10850). The jet is partially ionized, and ions move due to collisions with neutrals. Electrons support quasi-neutrality because of the electric field, which increases in inverse proportion to the distance along the field lines up to the jet. Behind the  $N_{0h}$  latitude, the electric field abruptly decreases, since the neutral density exponentially drops.

A displacement of the  $N_e$  maximum from the geomagnetic equator or the appearance of the second maximum is a common indicator of a TC with an intensity that is higher than the tropical storm intensity in the upper ionosphere. This phenomenon is related to an additional energy input into the ionosphere above a TC. After the evening (18, 19 LT) burst of the plasma drift vertical velocity (Heelis, 2004), this effect is especially pronounced, which is evident when the upper and lower parts of Fig. 3 are compared. This effect differs fundamentally from “the equatorial fountain” (Deminov, 2008). The stratospheric circulation and, correspondingly, the response of the ionosphere change for interacting TCs (Fig. 2b).

A local ascent, separated with respect to the sorts of atoms, of the neutral component in the ionosphere above an intense TC modifies ELF–VLF oscillations, since the ion components are responsible for the oscillation spectrum. The publications by Mikhailova et al. (2002) showed that the modification of the ELF–VLF oscillation spectrum observed on a satellite is the most sensitive indicator of the TC effect on the ionosphere. The lower hybrid oscillations with the  $\Omega_{lh}$  frequency are most intense in this range. On the Cosmos-1809 satellite, signals in the  $f=4600$  Hz channel with the  $f/8$  bandwidth under the TC Harry observation conditions include  $\Omega_{lf}$  oscillations if the oxygen concentration increases at 960 km altitude. A three-peak structure in the  $f=4600$  Hz channel is observed here in several successive orbits (Fig. 5). The first typical maximum is located in the geomagnetic equator region. The second maximum is projected along the geomagnetic field onto the region above the TC, where the motion of neutrals becomes free. The third maximum is projected onto the region of incident particles of the jet and boundary layer (Fig. 8). This is confirmed by the model of an additional input of neutrals above the TC and their transport by the east wind (Isaev et al., 2010).

## 2. Passage of TC Harry, New Caledonia.

An analysis, performed by the GPS interferometry method, of ionospheric disturbances above the largest hurricanes in 2004–2008 in the Atlantic Ocean indicated that strong turbulization and acoustic gravity waves (AGWs) are observed when a TC crosses Cuba, the Bahamas, and coastal regions (Zakharov et al., 2012; Zakharov and Kunitsyn, 2012). The plane of the Cosmos-1809 descending orbit on February 11, 1989, crossed the midnight sector. The disturbances observed in the upper ionosphere substantially depended on the TC and satellite relative position.

### (A) TC near the orbital plane, orbit 10864.

Flowing around the vertical structure (the stratospheric anticyclone plus a submerged jet), the east wind will incline this structure southward due to its deceleration by an island. If hydrogen atoms in a jet are injected with the most probable velocity at an angle of  $\sim 20^\circ$  with respect to the vertical, the data of all devices can be coordinated with the scheme proposed in Fig. 8.

The center of an additional narrow  $Ne$  peak will shift to  $L = 1.82$ , and the beginning of the peak will move to  $L = 1.65$ . The peak width is  $\sim 1200$  km, which is larger than such a width in orbit 10850 by a factor of 1.5. The  $Ne$  fluctuation intensity within the peak is lower than outside the peak, where  $\Delta Ne \sim 2\%$ , by a factor of 2–3.

A wide  $Ne$  maximum is located at  $L = 1.31$  and is projected along the geomagnetic field onto an altitude of  $\sim 230$  km above the TC center. Weak turbulence in the  $f = 450$  Hz channel is observed in the  $\sim 300$  km band along the satellite orbit above TC adjacent to  $L = 1.48$ . Such a situation can take place if the hydrogen ion

concentration decreases, which follows from Fig. 8. Correspondingly, oscillations will damp less intensely near the hydrogen cyclotron frequency. The TC center is surrounded by bursts in the  $f = 140$  Hz channel, where the intensity increases by a factor of  $\sim 2.5$ . We can anticipate that the helium ion concentration is decreased in these bursts, which should be confirmed experimentally.

Four similar peaks in the  $f = 140$  Hz channel with the same magnitude ( $\sim 300$  km) were registered in the magnetically conjugate region at  $1.48 \leq L \leq 1.82$ , and the peaks were located in density caverns. The fact that ELF oscillations are observed at one of the geomagnetic shells separated by the opacity barrier can be explained by ballistic wave propagation (Krasovskiy et al., 1983). Photoelectrons from the peak region can maintain such a relation. Electrons at the  $1.31 \leq L \leq 2.6$  shells are strongly disturbed since the spectrum in the  $f = 15$  kHz channel is turbulent.

The electric field with the northeastward horizontal component up to 10 mV/m and small-scale peaks in the vertical component reaching  $\sim 2$  mV/m is formed in the magnetically conjugate region at  $1.31 \leq L \leq 1.82$ .

This electric field does not change the electron gas pressure,  $P_e \approx 1$  nPa. The average pressure is  $P_e \approx 2$  nPa in the Southern Hemisphere up to  $45.17^\circ$  S ( $L = 3.39$ ) latitude, after which the satellite leaves the Earth's shadow.

The two regions discussed above are distinguished: the first at  $1.2 < L < 1.65$  with a diffused maximum at  $L = 1.31$  and the second at  $1.65 < L < 2.2$  with a maximum at  $L = 1.82$ .

### (B) TC before the evening terminator, orbit 10862.

An anomalous structure of the neutral component of the upper atmosphere above TC that crosses New Caledonia was clearly defined when the submerged jet top and descending branch were sunlit near the evening terminator. At that time, the satellite passed at  $\sim 45^\circ$  east of the island near the midnight meridian.

1. We define the following jet parameters:  $V_H$  is the neutral hydrogen velocity, and  $\beta$  is the angle of outflowing jet deviation from the vertical. We distinguish two regions in orbit 10862 in the Southern Hemisphere at  $L < 2.4$ , where the solar shadow is above the satellite. In the first region, rotating neutrals on the sunlit TC meridian will move along the geomagnetic field. Since ionization is increased, a burst of photoelectrons drifting eastward should be observed here. Correspondingly, we identify a burst at  $L = 2.1$  in the  $f = 140$  and 15 kHz channels (orbit 10862) with this burst. The geomagnetic field forms an angle of  $18.3^\circ$  with the vertical at this  $L$  shell on the TC meridian at 230 km altitude and  $\varphi_v = 33^\circ$  S latitude. For further estimations, we accept that  $\beta = 20^\circ$ .

The second disturbed region at  $1.65 < L < 1.95$  is related to the photoelectron drift from the region of

incidence of the jet and boundary layer neutrals. This region is centered at  $L = 1.75$ . On the TC meridian, this region crosses  $\varphi = 29.17^\circ$  S latitude, which bisects the central angle of average trajectories ( $\Delta\varphi$ ). An additional small  $Ne$  peak at  $L = 1.82$  coincides with the main peak in orbit 10864.

A neutral particle, which escapes and is incident at angle  $\beta$ , will fly along a spherical arc with radius  $R$  over the distance

$$s = \Delta\varphi R = \frac{R^2 V^2 \sin 2\beta}{g R_E^2}, \quad (5)$$

where  $R_E = 6370$  km is the Earth's radius,  $R = 6600$  km,  $g = 9.8$  m/s, and  $\Delta\varphi$  is the trajectory central angle.

On February 11 the satellite crossed the TC Harry zenith latitude at  $L = 1.48$ , which corresponds to the  $\varphi_0 = 21^\circ$  S escape latitude, and the geomagnetic shell  $L = 2.1$  is projected along the field line onto the  $\varphi_v = 33^\circ$  S entry latitude. Such particles should travel a distance of  $s_H = 1380$  km and have a velocity of  $V_H = 4400$  m/s, which corresponds to the atomic hydrogen temperature ( $T = 1170$  K).

In the spherical coordinate system, the vertex of a freely escaping particle parabola can be calculated using the formula

$$h = \frac{R^2 V^2 \cos^2 \beta}{2g R_E^2 - R V^2 \cos^2 \beta}. \quad (6)$$

Hydrogen atoms with the discovered parameters reach  $h = 1090$  km altitude, which is higher than the satellite altitude by 360 km. We assume that other atomic components of a neutral jet also escape from 230 km altitude with the same escape angles but with their own most probable velocities at the same temperature (1170 K). In such a case, oxygen and helium atoms will return to distances of  $s_O = 86$  km and  $s_{He} = 345$  km, respectively. We can assume that helium atoms form periodical structures in the boundary layer and excite acoustic waves in the lower ionosphere with the same magnitudes.

2. Electric field singularities in the situation when the evening terminator crosses TC.

If a periodic structure originates in the neutral jet density at altitudes of the lower ionosphere, a periodic electric field should appear at altitudes of the upper ionosphere when the ionization source is switched on/off (the terminator passes in our case). This effect can be observed from the satellite only in orbits that pass east of the TC meridian because of the eastward electron drift. Indeed, quasi-sinusoidal oscillations of the  $Ex$  and  $Ey$  field components with magnitudes about 350 km were registered in the sunlit ionosphere when the satellite left the shadow at 1056:47 UT. The intensity of VLF oscillations in the  $f = 4600$  Hz channel fluctuated synchronously with these oscillations up to the plasmopause ( $L = 4.5$ ). The plasma pressure ( $Pe$ ) growth intensified here up to  $L = 3.5$  with

increasing latitude, which is related to a linear increase in  $Ne$  and  $Te$  (a different inclination of dashed lines in Fig. 6 for orbit 10862). In these zones and only in this orbit, the intensity of the ELF noise magnetic component linearly increased in the H channel at  $f = 850$  Hz, the bandwidth of which includes the hydrogen cyclotron frequency in the lower ionosphere.

In the ionosphere partially illuminated by the scattered radiation at  $1.65 < L < 2.4$ , a less intense linear increase in  $Pe$  is only related to a linear increase in  $Ne$  at constant  $Te$ . Such a  $Pe$  behavior was registered in orbit 10863 with  $L = 1.82$  (this is marked by a dashed line on the adjacent panel). A displacement to higher  $L$  shells is caused by a shift of the geomagnetic equator at the satellite altitude by  $\sim 6^\circ$  N in orbit 10863 as a result of the geomagnetic dipole inclination, and the position of the geomagnetic equator in orbit 10862 coincides with the geographic position.

In the sunlit ionosphere of the Southern Hemisphere from the plasmopause to the polar oval, electric field oscillations are deformed and have shorter-wave components. They were observed only in orbits 10861–10864.

In magnetically conjugate regions of the Northern Hemisphere, similar phenomena were not observed when the satellite crossed these regions in the solar shadow. The electric field in orbits 10862–10864 and at  $1.31 < L < 2.2$  has the horizontal component, directed eastward toward the source, and the upward vertical component (some part of the  $Ey$  component). An anomalous  $Ey$  jump at  $48.1^\circ$  S is related to the fact that the satellite left the shadow at that time. Since a rod with an  $Ey$  sonde incompletely opened and a sonde was close to the satellite body, a potential jump of  $\sim 0.1$  V was observed in descending orbits at that time. Because of the Earth's rotation around the Sun, such an effect was observed a day before, when the satellite crossed a latitude of  $\varphi = 46.3^\circ$  S. A standard program for processing the electric field ignores this effect; therefore, such a jump is observed in Fig. 3 and in similar situations in the figures from (Isaev et al., 2010).

3. The effect of a VLF transmitter on the anomalous removal of neutrals above a TC.

It is known that fluxes of energetic charged particles are formed under the action of powerful VLF transmitters (Sonwalkar et al., 1994). In the nighttime ionosphere, these fluxes can be a pronounced source of additional ionization of the plasma neutral component. In orbit 10862 the satellite passed over an NPM transmitter with a power of  $\sim 0.5$  MW located on Hawaii. The effect of the neutral component additional ionization was observed in the Southern Hemisphere in the previous orbit (orbit 10863) when the geomagnetic declination was taken into account. An unusually high  $Ne$  concentration level at  $L = 1.2$  was also observed a day before in orbit 10849, when TC Harry did not reach New Caledonia and injected neu-

trals from a submerged jet vertically upward (Isaev et al., 2010).

B) TC after the morning terminator, orbits 10866–10868.

In the midnight sector west of Harry, the state of a disturbed ionosphere is complicated by powerful VLF transmitters after the satellite passage over the morning terminator. Figure 7 shows the instants when the satellite crossed the  $L$  shells, where the signals from the following transmitters were observed: Australian transmitters NST and NWC; Japan transmitter JJI; China transmitters 3SA and 3SB; Russian transmitters RA3 (Komsomolsk-on-Amur), RA1 (Novosibirsk), and RA2 (Krasnodar); and Indian transmitter VTX.

1. The solar shadow moves down below the  $Ne$  maximum above TC, orbit 10866.

The  $Ne$  fluctuations with a maximum at  $L = 1.82$  were observed at  $1.65 < L < 2.05$  in the Southern Hemisphere. In this case the electric field component about 5 mV/m, which was also centered at  $L = 1.82$  and directed along the geomagnetic field toward TC, was simultaneously registered in a wider region ( $\sim 15^\circ$ ). In this region in the  $f = 140$  Hz channel, the emission intensity before  $L = 1.82$  was twice as low as after  $L > 1.82$ . In the conjugate region at  $1.48 < L < 2.05$ , the oscillations intensified in the  $f = 450$  Hz channel, the bandwidth of which includes the hydrogen cyclotron frequency. Such a dependence, which is reproduced over  $\sim 60^\circ$  along longitude, may be related to the hydrogen ion drift. An additional singularity is that the electron density cavern with a width of  $\sim 150$  km and a depth of  $\sim 20\%$  and with an increased ELF–VLF emission level appeared at  $L = 1.6$ . Such a localization of all disturbances agrees with the hypothesis that neutrals are obliquely injected from the region above a TC into the upper ionosphere.

The next four singular domains observed in orbit 10866 are related to the additional effect of VLF transmitters on a disturbed ionosphere.

In the Northern Hemisphere, a disturbed region at  $2.05 < L < 2.41$  is formed by charged particle fluxes under the influence of the RA3 and NST transmitters. Both transmitters operate at frequencies slightly higher than 18 kHz, which are partially included into the  $f = 15$  kHz channel bandwidth. Figure 7 shows two very strong intensity bursts in the 15 kHz channel, a density ( $Ne$ ) and pressure ( $Pe$ ) trough, and a vertical electric field of  $\sim 7$  mV/m in the absence of the horizontal component ( $Ex$ ). An additional analysis of  $Te$  indicates that two small bursts are present at the cavern edges.

In the Southern Hemisphere, a similar cavern in  $Ne$  and  $Pe$  was observed at  $2.41 < L < 2.63$  between the zones of influence of NST and, apparently, RA1 transmitters. We should note that a similar singularity was observed on February 10 in orbit 10852.

Three solitons with decreasing amplitudes in the horizontal electric field move southward from the zone

of influence of two other transmitters 3SB ( $L \sim 1.44$ ) and NWC ( $L \sim 1.5$ ), which operate at frequencies slightly higher than 21 kHz. Since the transmitter working frequencies are shifted from the center frequency of the  $F = 15$  kHz channel, the transmitter signals are extracted weakly at 1745 UT.

The 3SA ( $L \sim 1.09$ ) transmitter, like the NPM, increases the  $Ne$  density of the nighttime equatorial ionosphere. At 1735 and 1742 UT, wide intensity bursts are registered in the  $f = 15$  kHz channel, since the satellite orbit passes near the geomagnetic equator ( $L \sim 1.07$ ). The region of latitudes with increased  $Ne$  is approximately twice as wide as the region in the previous (10865) and subsequent (10867) orbits. A similar pattern was also observed in this region on February 10, when neutrals were injected vertically.

2. The solar shadow approaches the TC magnetically conjugate region, orbit 10867.

Since a TC is intensified at night, neutral hydrogen additionally comes into the upper ionosphere, according to the proposed model. The concentration of hydrogen ions drifting westward should sharply increase when the morning terminator crosses the ionospheric region above a TC. On the Cosmos-1809 satellite, this effect can be found based on an increase in the lower hybrid frequency and a shift of these intense oscillations above the  $f = 4600$  Hz channel bandwidth. Indeed, a sharp, cone-shaped decrease in the signal intensity in the  $f = 4600$  Hz channel at  $1.41 < L < 1.9$  with a minimum at  $L = 1.6$  was registered only in orbit 10867 in the nighttime equatorial ionosphere. A sharp signal weakening in the  $f = 4600$  Hz channel with a similar width and depth was observed only in orbit 10853 a day before (on February 10), when the morning terminator passed over the TC. The cavern position shifted equatorward, since TC Harry only approached New Caledonia and a minimum bifurcated: one minimum was observed at  $L = 1.36$ , and another minimum, corresponding to the zenith above TC, was registered at  $L = 1.46$ .

Considerable fluctuations of the  $Ne$  density and emission intensity in the  $f = 140$  Hz and 15 kHz channels were observed in the conjugate region of the Northern Hemisphere. The passage of disturbances is apparently related to the electric field component along the geomagnetic equator and to three soliton structures of the  $Ne$  density directed toward the equator.

An analysis of ten ascending orbits that passed over the equator at local noon indicates that similar caverns at  $f = 4600$  Hz were observed only in orbits 10866 and 10867 in the Northern Hemisphere. A single cavern centered at  $L = 1.42$  ( $12.8^\circ$  N,  $270.4^\circ$  E) was registered in orbit 10867; three caverns centered at  $L = 1.25$  ( $4.8^\circ$  S,  $295.5^\circ$  E),  $1.36$  ( $7.2^\circ$  N,  $296.2^\circ$  E), and  $1.48$  ( $13.8^\circ$  N,  $296.2^\circ$  E) were registered in orbit 10866. A detailed analysis of the ascending orbits should be considered independently.

3. The region above a TC and the magnetically conjugate region after the terminator, orbit 10868.

The main singularity of the panel (orbit 10868) in Fig. 7 consists in the appearance of an additional  $N_e$  peak in the Northern Hemisphere at the same  $L$  shells ( $1.48 < L < 1.65$ ), when the TC magnetically conjugate region is behind the morning terminator. In the Southern Hemisphere,  $N_e$  increases at  $1.82 < L < 2.0$ . These regions are more pronounced in the electron gas pressure, since  $T_e$  rises here.

Only strong  $N_e$  fluctuations in the Northern Hemisphere at  $L = 1.86$  are registered in the next orbit (10869) with increasing distance from the terminator.

#### 4. CONCLUSIONS

A complex analysis of the Cosmos-1809 and Inter-cosmos-Bulgaria-1300 data during strong TCs made it possible to detect the following.

1. Additional plasma income into the upper ionosphere above isolated TCs and their dynamics.

2. Ionospheric precursors of cyclone intensification up to the hurricane stage in the form of local plasma density depression caverns above TCs. Such a precursor was previously observed as a result of a sharp increase in thunderstorm activity (Mikhailov et al., 2006; Price et al., 2009).

3. A shift of a wide plasma density maximum in the upper ionosphere from the geomagnetic equator into the region with the center projected along the geomagnetic field line up to 200–300 km altitudes at the TC latitude and the excitation of a wide lower hybrid oscillation band. This stage is typical of TCs reaching the intensity of categories I and II.

4. The injection of neutrals, which accompany the transition of a strong TC from category II to higher categories, into the upper ionosphere. TC intensification was previously registered as an abrupt change in the wave spectrum of the electron content in the ionosphere above the strongest hurricanes in 2004–2008 in the Atlantic water area (Zakharov et al., 2012).

#### ACKNOWLEDGMENTS

We are grateful to Professor P. Getsov and Professor V.D. Kuznetsov for the support of the work and to G.A. Mikhailova for a fruitful discussion.

#### REFERENCES

- Aburjania, G.D., Kharshiladze, O.A., and Chargazia, Kh.Z., Self-organization of IGW structures in an inhomogeneous ionosphere: 2. Nonlinear vortex structures, *Geomagn. Aeron.* (Engl. Transl.), 2013, vol. 53, pp. 759–760.
- Araujo-Pradere, E.A., Fuller-Rowell, T.J., and Bilitza, D., Validation of the storm response in IRI2000, *J. Geophys. Res.*, 2003, vol. 108A, p. 1120. doi 10.1029/2002JA009720
- Artekha, S.N., Gol'braikh, E., and Erokhin, N.S., On the role of electromagnetic interactions in the dynamics of powerful atmospheric vortices, *Vopr. At. Nauki Tekh.*, 2003, no. 4, pp. 94–99.
- Artekha, S.N., Belyan, A.V., and Erokhin, N.S., Manifestation of electromagnetic phenomena in atmospheric processes, *Sovrem. Probl. Dist. Zond. Zemli Kosmosa*, 2013, vol. 10, no. 2, pp. 225–233.
- Belyaev, G., Kostin, V., Trushkina, E., Ovcharenko, O., and Boichev, B., Variations in the ionospheric parameter when typhoons form and develop, *Proc. SES 2010*, Sofia, 2011, pp. 83–90.
- Belyaev, G., Bankov, N., Boychev, B., Kostin, V., Trushkina, E., and Ovcharenko, O., Observation of plasma oscillating structures in external ionosphere over cyclones, *SunGeo*, 2012, vol. 7, no. 1, pp. 51–55.
- Bondur, V.G., Pulnits, S.A., and Uzunov, D., Influence of large-scale atmospheric vortex processes on the ionosphere as exemplified by the Katrina hurricane, *Fiz. Osnovy Issled. Zemli Kosmosa*, 2008, no. 6, pp. 3–11.
- Danilov, A.D., *Populyarnaya aeronomiya* (Popular Aeronomy), Leningrad: Gidrometeoizdat, 1989.
- Danilov, A.D., Kazimirovskii, E.S., Vergasova, G.V., and Khachikyan, G.V., *Meteorologicheskie efekty v ionosfere* (Meteorological Effects in the Ionosphere), Leningrad: Gidrometeoizdat, 1987.
- Deminov, M.G., The Earth's ionosphere, in *Plazmennaya geliogeofizika* (Plasma Heliogeophysics), Moscow: Fizmatlit, vol. 2, pp. 92–163.
- Effects of thunderstorm activity on the upper atmosphere and ionosphere, *J. Atmos. Sol.–Terr. Phys.*, 1998, vol. 60, no. 7–9, pp. 667–973.
- Erokhin, N.S., Mikhailovskaya, L.A., and Shalimov, S.L., On the conditions of internal gravity wave propagation through wave structures from the troposphere into the ionosphere, *Geofiz. Protsessy Biosfera*, 2012, vol. 11, no. 4, pp. 5–22.
- Evtushenko, A.A. and Mareev, E.A., Modeling disturbances in the state of the mesosphere under the action of high-altitude discharges, i.e., sprites, *Izv. Vyssh. Uchebn. Zaved., Radiofiz.*, 2011, vol. 54, no. 2, pp. 123–140.
- Gabis, I.P. and Troshichev, O.A., The quasi-biennial oscillation in the equatorial stratosphere: Seasonal regularity in zonal wind changes, discrete QBO-cycle period and prediction of QBO-cycle duration, *Geomagn. Aeron.* (Engl. Transl.), 2011, vol. 51, pp. 508–519.
- Golitsyn, G.S., Polar lows and tropical hurricanes: Their energy and sizes and a quantitative criterion for their generation, *Izv. Atmos. Ocean. Phys.*, 2008, vol. 44, no. 5, pp. 537–547.
- Hanson, W.B., Coleg, W.R., Heelis, R.A., and Urguhart, A.L., Fast equatorial bubbles, *J. Geophys. Res.*, 1997, vol. 102A, pp. 2039–2046.
- Heelis, R.A., Electrodynamics in the low and middle latitude ionosphere: A tutorial, *J. Atmos. Sol.–Terr. Phys.*, 2004, vol. 66, no. 10, pp. 825–838.
- Hegai, V.V., Kim, V.P., and Illich-Svitych, P.V., The formation of a cavity in the night-time midlatitude ionospheric E-region above a thundercloud, *Planet. Space Sci.*, 1990, vol. 38, pp. 703–707.
- Holton, J.R., Curry, J.A., and Pyle, J.A., *Encyclopedia of Atmospheric Sciences*, London: Academic, 2003.

- Isaev, N.V., Kostin, V.M., Belyaev, G.G., Ovcharenko, O.Ya., and Trushkina, E.P., Disturbances of the topside ionosphere caused by typhoons, *Geomagn. Aeron.* (Engl. Transl.), 2010, vol. 50, pp. 253–264.
- Isaev, N.V., Sorokin, V.M., Chmyrev, V.M., Serebryakova, O.N., and Yashchenko, A.K., Disturbance of the electric field in the ionosphere by sea storms and typhoons, *Cosmic Res.*, 2002, vol. 40, no. 6, pp. 547–553.
- Ivanov, K.G., Generation of the Katrina hurricane during the geomagnetic extrastorm at crossing of the heliospheric current sheet: Is it an accidental coincidence or physical essence?, *Geomagn. Aeron.* (Engl. Transl.), 2006, vol. 46, pp. 609–615.
- Ivanov, K.G., Correlation between tropical cyclones and magnetic storms during cycle 23 of solar activity, *Geomagn. Aeron.* (Engl. Transl.), 2007, vol. 47, pp. 371–374.
- Kelley, M.S., Sietring, C.L., Pfaff, R.F., et al., Electrical measurements in the atmosphere and ionosphere over an active storm. 1. Campaign overview and initial ionospheric results, *J. Geophys. Res.*, 1985, vol. 90, pp. 9815–9823.
- Komrakov, G.P., Ivanov, V.P., Popkov, I.V., and Tyukin, V.N., Measuring the ionospheric electron density using the HF impedance probe method, *Cosmic Res.*, 1970, vol. 8, no. 2, pp. 278–283.
- Kostin, V.M., Belyaev, G.G., Ovcharenko, O.Ya., and Trushkina, E.P., Structural formations in the upper ionosphere caused by typhoons, *Tez. Konf. "Fizika plazmy v solnechnoi sisteme"* (Proc. Conference "Physics of Plasma in the Solar System"), IKI, 2011, p. 45.
- Kostin, V.M., Komrakov, G.P., Belyaev, G.G., Sobolev, Ya.P., Ovcharenko, O.Ya., and Trushkina, E.P., Nonlinear effects in the upper ionosphere during HF heating according to the Cosmos-1809 satellite data, *Sb. Tez. 8-ya konferentsiya "Fizika plazmy v solnechnoi sisteme"* (Proc. 8th Conference "Physics of Plasma in the Solar System"), IKI, 2013, p. 77.
- Krasovskiy, V.L., Kushnerevskiy, V.V., Migulin, V.V., Oraevskiy, V.N., and Pulinets, S.A., Ballistic wave transformation as a mechanism for the linkage of terrestrial kilometric radio waves with low-frequency noise in the upper atmosphere, *Geomagn. Aeron.*, 1983, vol. 23, no. 6, p. 702.
- Krivolutsky, A.A. and Repnev, A.I., Impact of space energetic particles on the Earth's atmosphere: A Review, *Geomagn. Aeron.* (Engl. Transl.), 2012, vol. 52, pp. 723–754.
- Landa, P.S., *Nonlinear oscillations and waves in dynamical systems*, Dordrecht: Kluwer Academic. Publ., 1996.
- Mikhailov, Yu.M., Druzhin, G.I., Mikhailova, G.A., and Kapustina, O.V., Thunderstorm activity dynamics during hurricanes, *Geomagn. Aeron.* (Engl. Transl.), 2006, vol. 46, pp. 825–839.
- Mikhailova, G.A., Mikhailov, Yu.M., and Kapustina, O.V., Variations of ULF–VLF electric fields in the external ionosphere over powerful typhoons in Pacific Ocean, *Adv. Space Res.*, 2002, vol. 30, no. 11, pp. 2613–2618.
- Molchanov, O.A., *Nizkочастотные волны i inducirovannyye izlucheniya v okolozemnoi plazme* (Low-Frequency Waves Induced in the Near-Earth Plasma), Moscow: Nauka, 1985.
- Price, C., Asfur, M., and Yair, Y., Maximum hurricanes intensity preceded by increase in lightning frequency, *Nature Geosci.*, 2009. doi 10.1038/ngeo477
- Pulinets, S.A., Hegai, V.V., Kim, V.P., Boyarchuk, K.A., and Lomonosov, A.M., Quasielectrostatic model of atmosphere–thermosphere–ionosphere coupling, *Adv. Space Res.*, 2000, vol. 26, no. 8, pp. 1209–1218.
- Rudenko, O.V. and Sapozhnikov, O.A., Interaction between wave beams containing shock fronts, *Usp. Fiz. Nauk*, 2004, vol. 165, no. 9, pp. 973–989.
- Sidorova, L.N. and Filippov, S.V., Longitudinal statistics of plasma bubbles observed as He<sup>+</sup> density depletions at altitudes of the topside ionosphere, *Geomagn. Aeron.* (Engl. Transl.), 2013, vol. 53, pp. 60–72.
- Smith, R.W., Vertical winds: A tutorial, *J. Atmos. Sol.–Terr. Phys.*, 1998, vol. 60, no. 14, pp. 1425–1434.
- Sonwalkar, V.S., Inan, U.S., Bell, T.F., Helliwell, R.A., Chmyrev, V.M., Sobolev, Ya.P., Ovcharenko, O.Ya., and Selegij, V., Simultaneous observations of VLF ground transmitter signals on the DE 1 and COSMOS 1809 satellites: Detection of a magnetospheric caustic and a duct, *J. Geophys. Res.*, 1994, vol. 99A, pp. 17511–17522.
- Sorokin, V.M. and Pokhotelov, O.A., The effect of wind on the gravity wave propagation in the Earth's ionosphere, *J. Atmos. Sol.–Terr. Phys.*, 2010, vol. 72, no. 2-3, pp. 213–218.
- Vanina-Dart, L.B., Pokrovskaya, I.V., and Sharkov, E.A., Response of the lower equatorial ionosphere to strong tropospheric disturbances, *Geomagn. Aeron.* (Engl. Transl.), 2008, vol. 48, 245–250.
- Vanina-Dart, L.B., Pokrovskaya, I.V., and Sharkov, E.A., Variations in the critical frequency of the ionospheric F2 layer according to tomographic sounding during the passage of a tropical cyclone, *Issled. Zemli Kosmosa*, 2011, no. 3, pp. 30–39.
- Veretenenko, S.V. and Pudovkin, M.I., Variations of total cloudiness during solar cosmic ray events, *Geomagn. Aeron.* (Engl. Transl.), 1996, vol. 36, pp. 108–111.
- Zakharov, V.I. and Kunitsyn, V.E., Regional features of atmospheric manifestations of tropical cyclones according to ground-based GPS network data, *Geomagn. Aeron.* (Engl. Transl.), 2012, vol. 52, p. 533.
- Zakharov, V.I., Kunitsyn, V.E., and Titova, M.A., Possibilities of determining surface sources of wave disturbances, identified in the ionosphere using the GPS interferometry methods, *Sb. Tezisov. 7-ya konferentsiya "Fizika plazmy v solnechnoi sisteme"* (Proc. 7th Conference "Physics of Plasma in the Solar System"), 2012, p. 67.

Translated by Yu. Safronov